THE AMERICAN SOCIETY OF MECHANICAL ENGINEERS
345 E. 47 St., New York, N.Y. 10017

91-GT-45

Three-Dimensional Flow Near the Blade/Endwall Junction of a Gas Turbine: Application of a Boundary Layer Fence

J. T. CHUNG, T. W. SIMON
Department of Mechanical Engineering
University of Minnesota
Minneapolis, MN 55455

and

J. BUDDHAVARAPU
TSI Incorporated
St. Paul, MN 55164

ABSTRACT

A flow management technique designed to reduce some harmful effects of secondary flow in the endwall region of a turbine passage is introduced. A boundary layer fence in the gas turbine passage is shown to improve the likelihood of efficient film cooling on the suction surface near the endwall. The fence prevents the pressure side leg of the horseshoe vortex from crossing to the suction surface and impinging on the wall. The vortex is weakened and decreased in size after being deflected by the fence. Such diversion of the vortex will prevent it from removing the film cooling flow allowing the flow to perform its cooling function. Flow visualization on the suction surface and through the passage shows the behavior of the passage vortex with and without the fence. Laser Doppler velocimetry is employed to quantify these observations.

NOMENCLATURE

C	chord
C_{pt}	total pressure coefficient, $(P_t-P_{tr})/(.5*\rho U_o^2)$
H	height of the fence
P	pitch
P_t	total pressure
P_{tr}	total pressure in freestream upstream of the cascade
Re_c	Reynolds number based on chord, U_oC/ν
$Re_{\delta 2}$	Reynolds number based on momentum thickness, $U_o\delta_2/\nu$
U_o	inlet velocity
v	resolved cross-stream component
w	resolved spanwise component
w1	velocity component measured by LDV in 16.5° tilted plane
w2	velocity component measured by LDV in 61.5° tilted plane
x	streamwise coordinate
y	cross-streamwise coordinate
z	spanwise coordinate
δ_2	momentum thickness

INTRODUCTION

The demand to improve the efficiency of modern gas turbines has led to continued increases in jet engine turbine inlet temperature. Higher inlet gas temperatures generally subject the blades or vanes to a more severe environment as airfoil temperatures and thermal stresses rise and yield strength falls. Thus, though an increase in the turbine inlet temperature increases propulsion efficiency, it can reduce component life significantly. Some gains in allowable component temperature are obtained by improvements in existing materials and development of new materials. However, most of the increases in the inlet temperature have resulted from improved cooling schemes for the airfoils. Surface film cooling, for which coolant air is injected into the gas stream through holes on the blade or the endwall surface, has been effective in reducing the overall surface temperatures. The effectiveness of this scheme depends on an accurate prediction of near-wall flow direction and minimal near-wall mixing. However, secondary flows near the airfoil/endwall junction decrease the certainty of local flow direction and contribute to enhanced mixing. Modern gas turbines tend to have progressively smaller aspect ratios and hence, progressively larger regions on the blade surface which are influenced by the strong endwall secondary flow. Because of this trend, (1) secondary flows are becoming more important, (2) knowledge of the effects of secondary flows on the blade and endwall surface heat transfer and on film cooling performance is becoming more crucial and (3) interest in modifying the endwall flow has intensified.

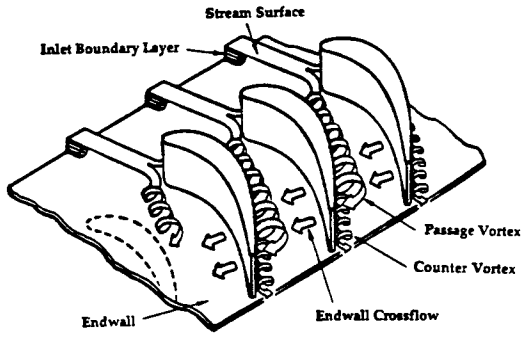

Fig. 1 Endwall secondary flow model after Langston (1980).

Details about the secondary flow field in turbine passages have been reported by Langston et al. (1977), Graziani et al. (1980), Sieverding (1985) and Goldstein and Spores (1988). Various flow visualization results taken from turbine cascades were shown by Herzig et al. (1954), Sieverding and Van den Bosche (1983) and Chung and Simon (1990). The flow in the turbine passage is complex, containing two legs of a horseshoe vortex, a passage vortex, a saddle point on the endwall, liftoff of the passage vortex, endwall crossflow and flow reattachment on the suction surface of the blade (Fig. 1). The passage

Presented at the International Gas Turbine and Aeroengine Congress and Exposition
Orlando, FL June 3-6, 1991

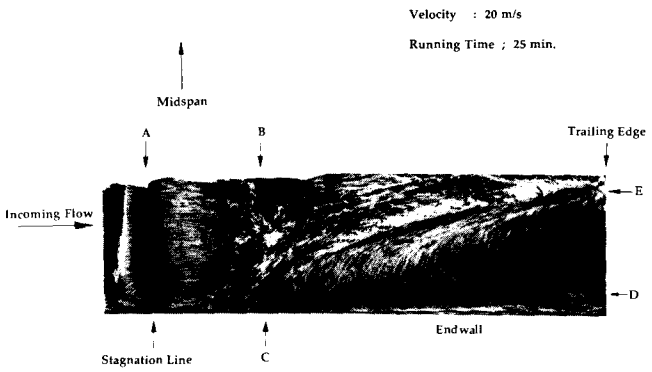

Fig. 2 Visualization of the three-dimensional flow on the suction wall near the endwall as revealed by the oil and lampblack technique (from Chung and Simon, 1990).

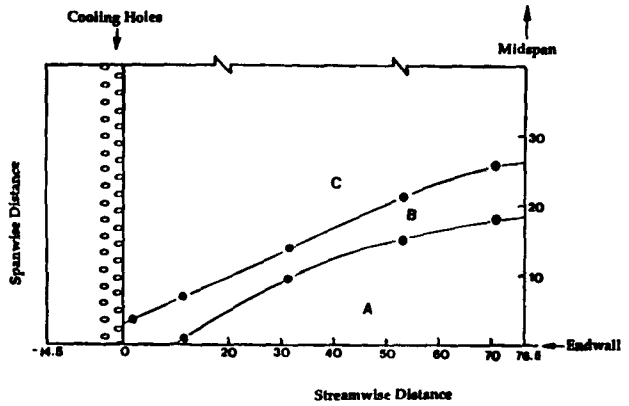

Fig. 3 Distribution range of average film cooling effectiveness in the endwall region on the suction surface of a blade (from Chen, 1984).

of both legs of the horseshoe vortex and the low momentum flow (new endwall boundary layer) adjacent to the endwall are strongly influenced by the pressure gradient established across the passage due to the mainflow curvature.

The effects of the secondary flow on the surface heat transfer to the endwalls and airfoils have been documented by Graziani et al. (1980) and Goldstein and Spores (1988). They observed that the complex secondary flows in the endwall region of the turbine passage provide unwanted heat transfer augmentation on the endwall and suction surfaces of the airfoil. Secondary flows apparently have little influence on heat transfer to the pressure side surface of the airfoil; the flow pattern is almost two-dimensional. One particularly troublesome aspect of heat transfer enhancement to the blade comes about as the passage vortex impinges upon the suction wall of the airfoil, then lifts off the endwall, rising on this surface while increasing in size as shown in Fig. 2, a visualization of the wall shear on the suction surface near the endwall (Chung and Simon, 1990). The passage vortex impinges upon the suction wall at C and then climbs the wall while proceeding downstream, arriving at elevation E at the trailing edge.

The film cooling performance on the surface of the blade near the endwall is influenced by this secondary flow. Film cooling effectiveness on a gas turbine blade near the endwall was investigated by Goldstein and Chen (1985) using a single row of injection holes and by Goldstein and Chen (1987) using two rows of injection holes. They found a triangular shaped region on the suction surface of airfoils where the flow field created by the secondary flow washes film cooling air away from the surface reducing the film cooling effectiveness to essentially zero. Figure 3 from Chen (1984) shows ranges of average effectiveness on the suction surface of a blade. Region A is an unprotected region where the coolant flow is swept away from the surface by the pressure-to-suction-surface secondary flow and the effectiveness is essentially

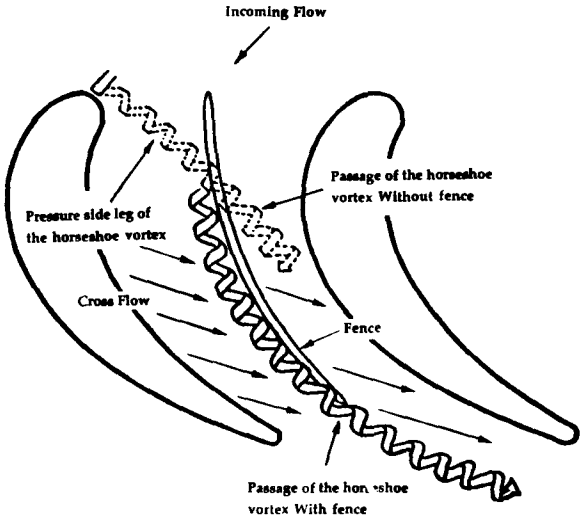

Fig. 4 Secondary flows in the endwall region with and without fence.

zero. Region B is a transition region, protected by the coolant but with an average film cooling effectiveness which is lower than that of the two-dimensional flow region above Region C. Takeishi et al. (1989) showed the effects of the three-dimensional flow field on heat transfer and the film cooling on the endwall, suction, and pressure surfaces of an airfoil using a low speed, annular vane cascade. They also observed the triangular region of reduced film cooling effectiveness.

These results motivate one to consider a means of reducing this effect by flow management techniques, attempting to reduce the harmful effects of the secondary flow field without adversely affecting other flow characteristics of the passage. Figure 4 shows the path of the pressure side leg of the horseshoe vortex (dotted-line vortex) across the passage, merging with the passage vortex, then impinging upon the suction surface of the airfoil and washing the triangular region shown in Figs. 2 and 3. It also shows cross flow which is due to the pressure gradient. It is of value to change the path of this vortex so that its impinging on the suction surface is reduced or prevented.

The present paper is based on the presumption that this secondary flow can be managed by placing a blockage to the flow, a fence, in the path of the vortex. The solid-line vortex in Fig. 4 shows the path of the pressure side leg of the horseshoe vortex when it is deflected by the fence into the high velocity channel flow. The vortex lifts as it climbs over the fence and is swept downstream by the freestream. It is thus assumed that the fence prevents the passage vortex from impinging upon the wall. It is assumed that this will reduce the washing of film cooling flow away from the endwall thus allowing film cooling flow to perform its function in this region. Kinnear et al. (1980) introduced an invention which, at first glance, appears to be similar. They fabricated an elongated step structure on the endwall shown in Fig. 5 for which the upstream edge acts as a vortex generator. This new vortex is to intercept and entrain the low momentum secondary flow traveling from the pressure side to the suction side and, thus, reduce the secondary flow in the endwall boundary layer. No mention was made by the authors of the horseshoe vortex. The intent of the present study is different. Here, no new vortex is intentionally formed. The fence is to deflect the horseshoe vortex into the freestream. Particular attention is paid to the trailing edge region on the suction surface of the blade near the endwall where thermal damage due to hot gas flow is most serious. The experiment to evaluate this scheme was performed on a large-scale cascade simulator described by Chung and Simon (1990). Flow visualization on the suction surface and through the passage was done with ink and oil of wintergreen (Langston and Boyle, 1982) and with a tuft grid. A single tuft probe (Chung and Simon, 1990) was used to observe the flow pattern on the endwall near the saddle point. The total pressure coefficients were measured near the junction of the endwall and the suction surface to examine the extra losses that may be present due to the fence. Laser-Doppler velocimetry was used to

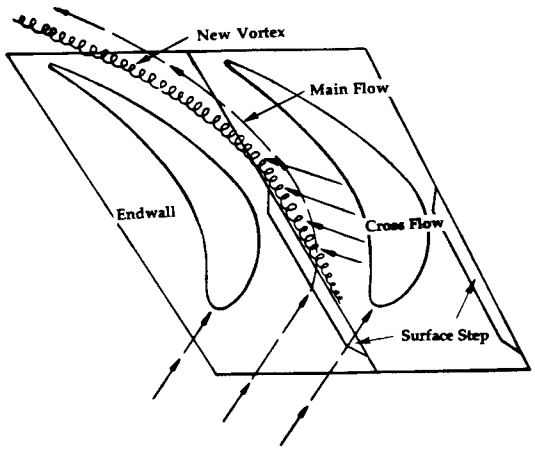

Fig. 5 The location of the step on the endwall between a pair of guide vanes (from Kinnear et al., 1980).

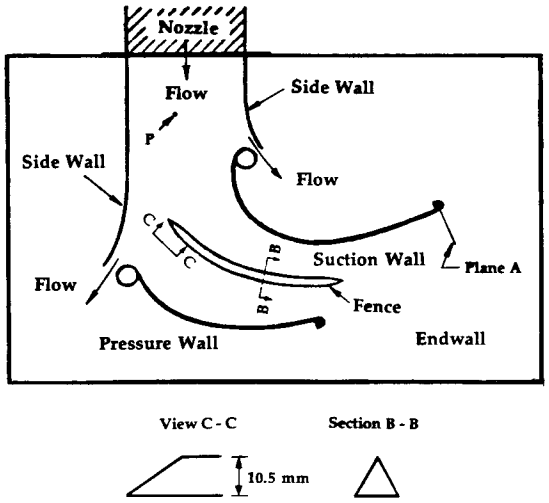

Fig. 6 Top view of the simulator, with the fence.

quantify these observations with measurements of the mean velocity components on a plane which is perpendicular to the surface of the airfoil.

EXPERIMENTAL APPARATUS AND PROCEDURE

1. Test Section and Test Conditions

The experiments were carried out in a low velocity wind tunnel which is a blown-type configuration exhausting to the atmosphere by passing through the test section, a large-scale cascade simulator. The blade profile of the test section is of the CF6-50 shape with chord length and height of 231 mm and 610 mm, respectively. The aspect ratio is 2.64 and the solidity ratio (chord/pitch) is 1.3. The angle of inlet and outlet flows are 44.3° and 62.7°, respectively. The diameter of the leading edge of the blade is 25.4 mm. Lexan sheets of 0.6 mm thickness are used for the pressure and suction walls. These pieces are attached to two plexiglass forms shaped to the blade profile. A top view of the simulator test section, which consists of two half-blades and two side walls is shown in Fig. 6. It does not show the forms at the ends of the blades. More details of construction and a description of the qualification of the simulator are presented by Chung and Simon (1990).

The experiments in this study were conducted at two velocities. The flow visualization was at a higher velocity to match the Reynolds number of a real gas turbine as closely as possible. The velocity for the LDV measurement was reduced somewhat to improve seeding. The test conditions are as follows :

Parameter	LDV measurements	Flow Visualization	
U_0	14.0	20.0	m/s
Re_c	2.05×10^5	2.93×10^5	
Displacement thickness+	1.7	2.6	mm
Shape Factor+	1.479	1.488	
$Re_{\delta 2}$+	1005	2162	
δ_2/H	0.11	0.165	
δ_2/C at the leading edge	0.0067	0.0090	

+ : For the inlet endwall boundary layer.

The momentum thickness of the inlet boundary layer on the endwall was measured by traverse of a total pressure tube 18 cm directly upstream of the left-hand side blade and somewhat nearer the nozzle center (point P of Fig. 6). The last two parameters of this list, δ_2/C and δ_2/H, were extrapolated from these measurements to the location of the leading edge of the left-hand side blade (by assuming flat plate, zero pressure gradient, boundary layer growth).

2. Instrumentation

A two-component fiberoptic laser Doppler velocimetry (LDV) system manufactured by TSI Inc. was utilized for the mean velocity measurement. The system consists of a "Colorburst" transmitting optical module, a "Colorlink" receiving module, IFA-550 signal processors, "FIND" data analysis software and an 83 mm diameter fiber optic probe. Frequency shifting (for flow reversal measurement) was available for each component. The receiving optical/electronic module provided filtering, color separation, photo-multiplication and frequency shifting. Auto-correlation of zero crossing of a Doppler signal was used to validate signals over noise (Jenson et al., 1988). The probe focal length was 250 mm and scattered light was collected in the backward scatter mode. A glycerin-water mixture (1 part glycerin in 3 parts of water) was used for particle seeding. It was the best of the several seeding schemes tried (incense and an atomized sugar/water solution). Compressed air was provided to a 6 jet atomizer (TSI model 9306) to derive the particles. The mixture was supplied ahead of the axial fan of the air supply system (only the nozzle of which is shown in Fig. 6).

Two normal velocity components were taken at a time, one in each of the two planes formed by the four beams of the two color system. The probe was located with its axis in the plane of the secondary flow vectors of Fig. 10, as shown in Fig. 7(a). In this configuration, the streamwise velocity component and a velocity component on this plane but perpendicular to the probe face were measured. In order to obtain the spanwise and cross-stream velocity components, the probe was tilted at two angles, 16.5° and 61.5°, with respect to the endwall, in this plane. Figure 7 shows the coordinate systems for each configuration in the measuring plane. These angles were chosen in order to provide measurements near the junction of the suction wall and the endwall, as well as to obtain good resolution of the velocities. Two sets of data (two angles) were taken at each point in the plane from which the spanwise and cross-stream components were calculated. The fiberoptic probe was traversed by a two-dimensional auto traversing device having 0.01 mm resolution in each direction which was controlled by a personal computer through the FIND data analysis software.

3. Configuration of the fence

The main objective of this study is to block and change the track of the pressure side leg of the horseshoe vortex. To do this, a fence was made of clay to an equilateral triangle shape of 13 mm on aside (Fig. 6). The 203 mm long fence had a gradual inclination on the leading edge, designed to reduce the strength of any extra vortex that may tend to form at the leading front. The fence was placed on the endwall to be in the path of the pressure side leg of the horseshoe vortex, as shown in Fig. 4. There is of course no special reason for this particular orientation. It is one of many arrangements that could have been tested. No attempt was made to optimize the geometry.

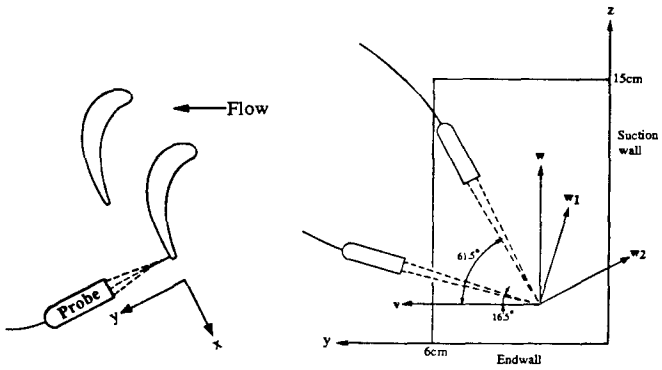

(a.) Top View (b.) Measuring Plane

Fig. 7 Coordinate systems for the LDV measurement.

4. Flow visualization

Flow visualization was used to observe the change of the secondary flow with the addition of the fence. The ink-dot-liquid-film technique introduced by Langston and Boyle (1982) was applied on the suction side surface of the blade near the endwall. The technique provides records of shear stress directions on the surface.

A tuft grid of 8 cm by 20.5 cm was utilized to observe the behavior of the vorticity within the passage. The assembly is composed of fishing line constructed in a rectangular grid with tufts connected, with loops, to each intersection. The tufts, yarn filaments of 2 cm length are free to point in the direction of the flow.

A single tuft probe, a thin rod with a single tuft tied with a loop at the end, was used to observe the flow pattern on the endwall within the saddle point region. A set of arrows was drawn on a grid map to match the observed tuft directions at each of the chosen positions. The composite shows the flow pattern.

RESULTS AND DISCUSSION

The tuft grid shows the sense of rotation and the evolution of the vortex as it passes through the simulator passage (Fig. 8). The figure displays the passage vortex near the trailing edge of the suction wall before the fence had been installed. Note that near the trailing edge, the center of the vortex has lifted away from the endwall and the diameter of the vortex is large. Several near-wall tufts are shown to rise steeply, indicating a highly skewed flow. Locating this grid at several streamwise positions allows tracking the vortex and monitoring its size. From these separate position measurements (not shown), one sees that the vortex is growing and climbing the suction surface. This behavior is in good agreement with Fig. 1. Figure 9 shows the secondary flow pattern at the same streamwise station but with the fence in place. The center of the vortex which was clear in Fig. 8 is less easily identified in this case. Also, the vortex seems to be nearer the endwall and the center of the channel (farther from the suction surface). This change due to the presence of the fence is also visible in Fig. 10, a plot of the secondary flow vectors measured with the LDV. The centers of the vortex is marked using + signs. These plots were obtained by calculating the in-plane spanwise and cross-stream components of the measured velocities, and for each cross-stream location, subtracting the components in the 2-D flow, which were very small in this plane. Points A and B, representing where the secondary flow components are maximum for each case, will be discussed later. The arrows show that the counterclockwise rotation of the secondary flow is stronger without the fence than with the fence. Apparently the vortex which has been diverted into the freestream has either not been allowed to grow to the same strength or has dissipated more with the fence in the flow than without. The distance from the suction wall to the center of the vortex in Fig. 10 matches the distance from the suction wall to the downstream end of the fence in Fig. 6. One surmises that, as the vortex is lifted by the fence, it merges with the high momentum mainstream flow and turns downstream. When it rises and its axis begins to align with the freestream, it no longer is able to use the velocity gradient of the

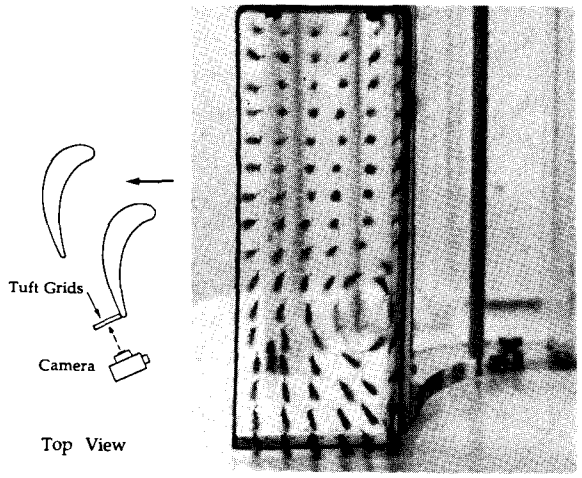

Fig. 8 Passage vortex at Plane A, without fence, as visualized by a tuft grid.

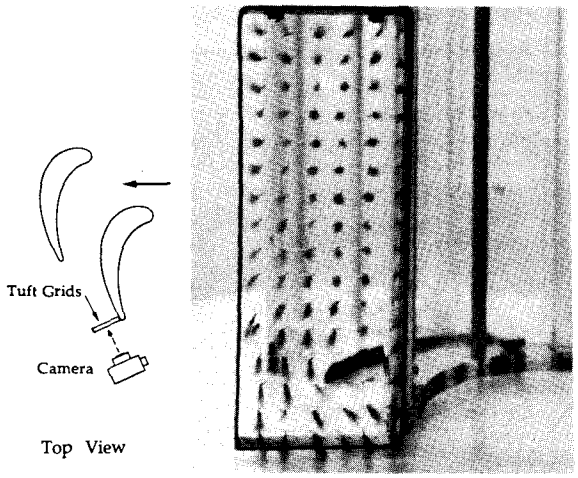

Fig. 9 Secondary flow pattern at Plane A, with fence, as visualized by a tuft grid.

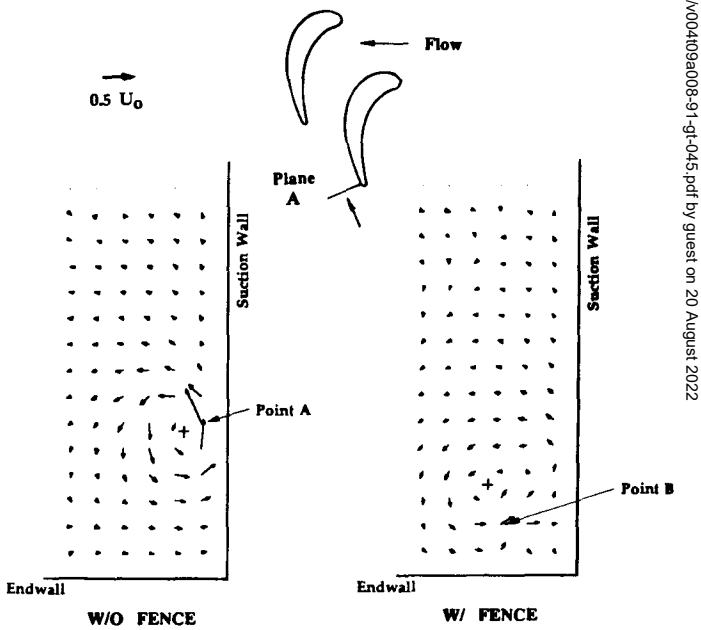

Fig. 10 Secondary flow vectors at plane A with and without fence.

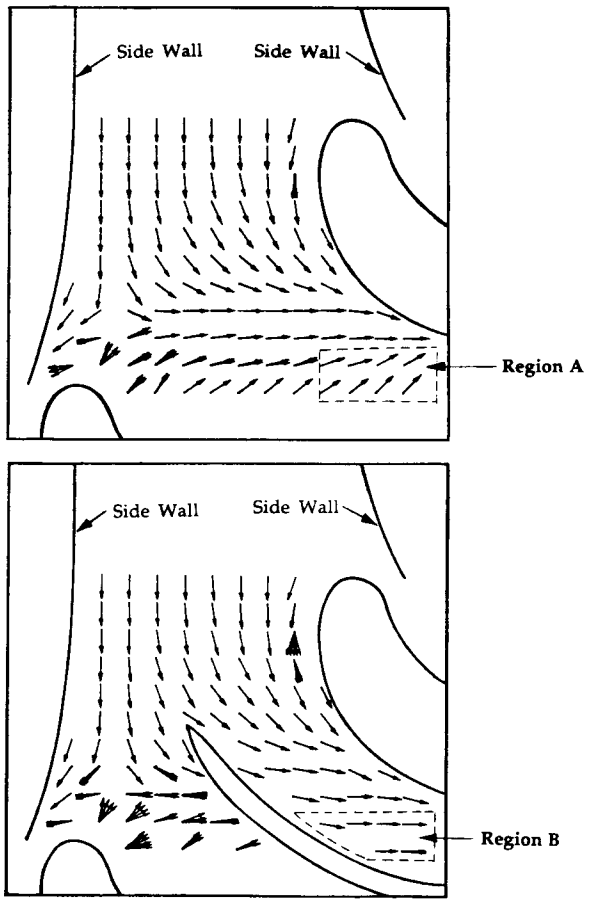

Fig. 11 Plots of directions of local shear stress on the endwall with and without the fence.

skewed endwall boundary layer to produce additional circulation. Thus, its growth is retarded. Secondly, it may be dissipating more rapidly as it interacts with the freestream, perhaps aided by the intensification and concentration of its vorticity as it experiences acceleration to the mainflow velocity and accelerates with the mainflow. The vortex is very weak, as shown in Fig. 10.

One must recognize that the facility employed was a simulator and not a true cascade. A question may arise, for instance, concerning the effect of interaction of the flow from outside the passage with the flow through the passage downstream of the pressure surface. From measurements and visualization, the authors can conclude that this interaction has little effect on the pressure-side horseshoe vortex trajectory and strength. Thus, the qualitative description of the effect of the fence is accurate though finer details of the flow downstream of the pressure side of the channel may not be correct.

Plots of directions of local shear stress on the endwall produced by using the single tuft probe (Chung and Simon, 1990) are shown in Fig. 11. Note that each arrow represents the direction, not the magnitude, of the shear stress. Multiple arrows at a single position indicate the unsteadiness of the flow. It is observed that the flow pattern upstream of the leading edge of the left-hand side blade is not noticeably affected by the fence. One notes that on the right-hand side, region A, there is a very highly skewed motion on the endwall due to the horseshoe vortex. This disappears when the fence is installed since the vortex is deflected (see region B). The arrows in this area still show the cross flow from the pressure side to the suction side, however, with and without the fence. Changes on the heat transfer pattern on the suction wall and the endwall due to the fence (with and without the film cooling) remain to be studied.

Figure 12 and Figure 13 produced by the ink and oil of wintergreen technique show shear stress directions on the suction surface with and without the fence in the passage. The mild skew in region A of Figs. 12

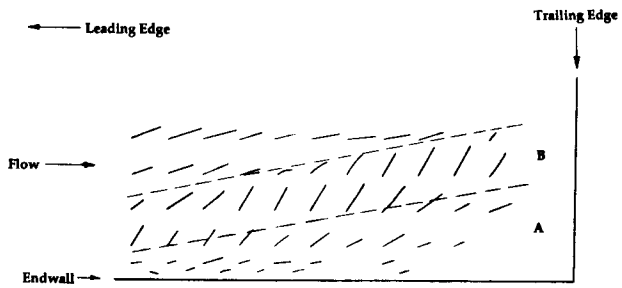

Fig. 12 Flow visualization on the suction wall near the endwall as revealed by the ink dot technique, without fence.

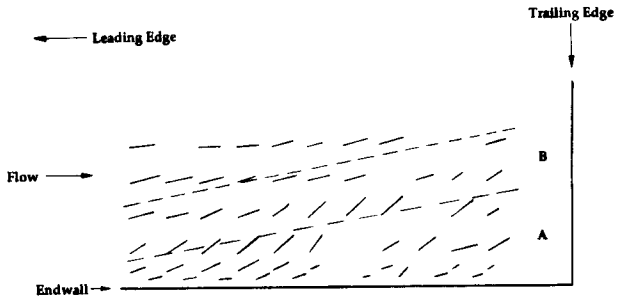

Fig. 13 Flow visualization on the suction wall near the endwall as revealed by the ink dot technique, with fence on the endwall.

and 13 is due to the secondary flow established in the curved channel which climbs the suction surface. This flow is common to curved channels and is not peculiar to turbine cascades. It is a continuation of the cross flow seen on the endwall on the right-hand side of the fence in Fig. 11. It appears that this flow pattern is unaffected by the fence and is not associated with the horseshoe vortex. This area could be protected by film cooling fluid supplied on the endwall surface. On the other hand, the highly skewed lines of region B in Fig. 12 represent the region where the passage vortex influences the suction sidewall flow. Langston et al. (1977) also showed this pattern. Because of the presence of the passage vortex, it would not be possible to film cool this region effectively by judicious choice of fluid injection position. This flow skewing is greatly reduced by the fence, as shown in Fig. 13. The changes on the suction surface and endwall surface of the airfoil support the observations presented along with Fig. 8 through Fig. 10. With the fence, the passage vortex is not allowed to reach the suction sidewall of the airfoil. Instead, it merges with the higher-momentum mainstream and remains in that stream.

The distribution of total pressure in the flow was measured to determine if any extra losses arise due to the fence. Figure 14 shows the distribution of the total pressure coefficient, Cp_t, which is defined as the difference between the local total pressure and the total pressure of the flow upstream of the cascade normalized by the velocity head upstream of the cascade. It shows a very high loss region near the suction surface for the case without the fence. This is some distance from the endwall, and where previous figures would indicate the vortex to be. Yamamoto (1987) also observed a high-loss core near the wall and noted that the passage vortex was the source. The high-loss region moves down and away from the suction surface when the fence is placed in the passage as shown in the right-hand plot of Fig. 14. The losses are much lower than those for the case without the fence. The average value of the change in total pressure across the measurement area (in Fig. 14) with the fence is -0.05 ; it is -0.12 without the fence. The reduced aerodynamic losses may be because the fence reduced the length of the vortex trajectory in which it resided in the boundary layer, moving nearly perpendicular to the mainstream flow (pictured as dotted vortex in Fig. 4). It is felt that the vortex grows and increases substantially in circulation in this region, extracting momentum from the mainflow at the upper reaches of the skewed endwall boundary layer. Another interesting contrast is in the kinetic energy of the

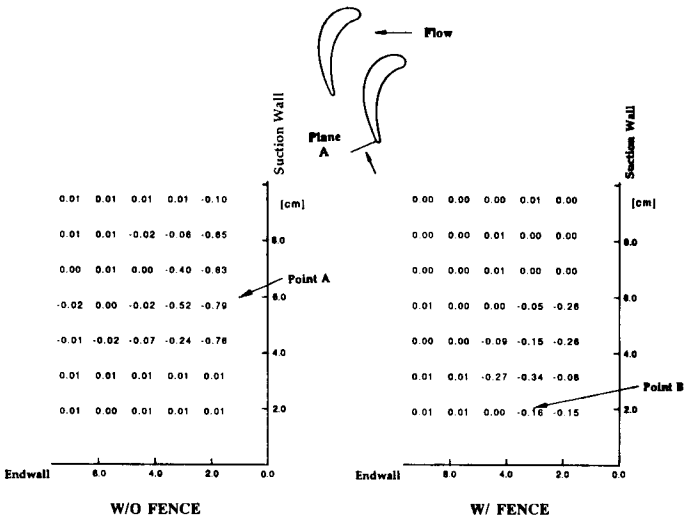

Fig. 14 Total pressure loss distributions at plane A normalized by the velocity head upstream of the cascade (with and without the fence).

vortex, presented as the square of the secondary flow components of velocity (component seen on Fig. 10) normalized by the velocity head upstream of the cascade. For instance, the magnitude of this ratio at point A in Fig. 10 is -0.361. This is the maximum value measured without the fence -- a much larger value than those taken with the fence. The total pressure coefficient similar to those of Fig. 14, at the same point is -0.562. Since this rotational kinetic energy is not converted to mechanical energy downstream -- it is merely dissipated -- it represents an additional loss. Therefore, the total dimensionless loss at this point is -0.923. When the fence is placed in the passage, the maximum vortical kinetic energy coefficient is only -0.034 (at the point B in Fig. 10). The total pressure coefficient at this point is -0.045 so the total loss is -0.079. It confirms that the presence of the fence in the passage not only improves the opportunities for cooling the suction wall with film cooling but also reduces hydrodynamic losses.

SUMMARY AND CONCLUSION

In the present study, a secondary flow control technique which employed a fence was introduced into a cascade simulator. Comparisons of the flow patterns made by flow visualization and LDV measurements show that the fence on the endwall is valuable in keeping the passage vortex from impinging on the suction wall. As a result, the film cooling performance on the suction wall near the endwall can be improved and losses can be reduced. Conclusions drawn from this study are :

1. At the trailing edge of the suction surface where the vortex flow is problematic, the horseshoe vortex is brought nearer the endwall and farther from the suction surface by installation of the fence.

2. The highly skewed motion on the suction surface near the endwall due to the passage vortex can be reduced by a fence on the endwall.

3. The strength of the vortex flow is reduced by the presence of the fence.

4. The presence of the fence appears to reduce aerodynamic losses associated with the endwall secondary flow.

ACKNOWLEDGEMENTS

This study was supported by the Air Force Office for Scientific Research under grant number F49620-85-C-0049. The grant monitor was Captain Hank Helin. Further support was provided by the Graduate School of the University of Minnesota.

REFERENCES

Chen, P. H., 1984, "Film Cooling of a Turbine Blade by Injection Through Two Rows of Staggered Holes in Near-End-Wall Region," M.S.M.E. Thesis, Department of Mechanical Engineering, University of Minnesota, Minneapolis, MN.

Chung, J. T. and Simon, T. W., 1990, "Three-Dimensional Flow near the Blade/Endwall Junction of a Gas Turbine: Visualization in a Large-scale Cascade Simulator," ASME paper 90-WA/HT-4, Presented at the Winter Annual Meeting.

Goldstein, R. J., and Chen, H. P., 1985, "Film Cooling on a Gas Turbine Blade near the End Wall," ASME *Journal of Engineering for Gas Turbines and Power*, Vol. 107, pp. 117-122.

Goldstein, R. J., and Chen, P. H., 1987, "Film Cooling of a Turbine Blade with Injection Through Two Rows of Holes in the Near-Endwall Region," ASME *Journal of Turbomachinery*, Vol. 109, pp. 588-593.

Goldstein, R. J., and Spores, R. A., 1988, "Turbulent Transport on the Endwall in the Region Between Adjacent Turbine Blades," ASME *Journal of Heat Transfer*, Vol. 110, pp. 862-869.

Graziani, R. A., Blair, M. F., Taylor, J. R., and Mayle, R. E., 1980, "An Experimental Study of Endwall and Airfoil Surface Heat Transfer in a Large Scale Turbine Blade Cascade," ASME *Journal of Engineering for Power*, Vol. 102, pp. 257-267.

Herzig, H. Z., Hansen, A. G., and Costello, G. R., 1954, "Visualization Study of Secondary Flow in Cascades," NACA TN 1163.

Jenson, L. M., Menon, R. K., Miller, J. D., and Fingerson, L. M.,1988, "An Automatic Signal Processor for LDV Systems," FlowLines, TSI Incorporated, St. Paul, MN.

Kinnear, I. S., May, A. L., and Wall, R. A., 1980, "Secondary Flow Control in Axial Fluid Flow Machine," UK Patent Application GB 2 042 675 A.

Langston, L. S., Nice, M. L., and Hooper, M. R., 1977, "Three-Dimensional Flow Within a Turbine Cascade Passage," ASME *Journal of Engineering for Power*, Vol. 99, pp. 21-28.

Langston, L. S., 1980, "Crossflows in a Turbine Cascade Passage," ASME *Journal of Engineering for Power*, Vol. 102, pp. 866-874

Langston, L. S., and Boyle, M. T., 1982, "A New Surface-Streamline Flow Visualization Technique," *Journal of Fluid Mechanics*, Vol. 125, pp. 53-57.

Sieverding, C. H., and Van den Bosche, P., 1983, "The Use of Coloured Smoke to Visualize Secondary Flows in a Turbine-Blade Cascade," *Journal of Fluid Mechanics*, Vol. 134, pp. 85-89.

Sieverding, C. H., 1985, "Recent Progress in the Understanding of Basic Aspects of Secondary Flows in Turbine Blade Passages," ASME *Journal of Engineering for Gas Turbines and Power*, Vol. 107, pp. 248-257.

Takeishi, K., Matsuura, M., Aoki. S., and Sato, T., 1989, "An Experimental Study of Heat Transfer and Film Cooling on Low Aspect Ratio Turbine Nozzles," ASME *Journal of Turbomachinery*, Vol. 112, pp. 504-511.

Yamamoto, A., 1987, "Production and Development of Secondary Flows and Losses in Two Types of Straight Turbine Cascade: Part 1 - A Stator Case," ASME *Journal of Turbomachinery*, Vol. 109, pp. 186-193.